

Velocity-tuned resonances and resonance fluorescence in a standing-wave field

G. S. Agarwal

School of Physics, University of Hyderabad, Hyderabad 500 134, India

Yifu Zhu

Schlumberger-Doll Research, Ridgefield, Connecticut 06877

(Received 9 January 1992)

The dynamics of quantum fluctuations in an atom interacting with a standing-wave field is studied. The spectrum of resonance fluorescence is calculated using a formulation based on optical Bloch equations for two-time correlation functions and continued-fraction methods. The spectra are calculated both under resonant and nonresonant conditions. The resonance condition in the context of a standing-wave field corresponds to a velocity-tuned or Doppleron resonance that in turn depends on the intensity of the pump. The Doppleron resonances are extracted from the positions of maxima in the total intensity of fluorescence. The spectral features are explained in terms of the eigenvalues of the appropriate "Floquet" matrix.

PACS number(s): 42.50.Hz, 42.50.Lc, 42.50.Vk

I. INTRODUCTION

The quantum dynamics of an atom in an intense standing-wave electromagnetic field is extremely rich with many interesting consequences. Considerable work on this subject has been done in connection with electromagnetic forces on atoms. The multiphoton absorption from the two components of the standing wave leads to a number of resonances in observable properties such as fluorescence [1-3]. Consider multiphoton processes for a Doppler-broadened two-level system. The atom is affected by two traveling waves Doppler shifted in opposite directions. The nonlinear processes involving $(l+1)$ photons from one wave and l photons from the other wave produce resonance at the velocity

$$v = \pm \frac{\omega_0 - \omega_l}{(2l+1)k_l}, \quad (1.1)$$

where ω_0 is the atomic frequency, and ω_l and k_l are the frequency and wave vector of the standing wave. The position of the multiphoton resonance is shifted by the intensity of the field [3]. Kyröla and Stenholm [2] included the effects of atomic relaxation and calculated the excited-state population as a function of the velocity. For increasing intensity they found that the velocity-tuned or Doppleron resonances are shifted and new ones appear. There have been two recent measurements [4,5] of the Doppleron resonances. The experiments measure the fluorescence produced by a beam of excited atoms in the field of a standing wave. The fluorescence is monitored using a third beam. These experiments demonstrated Doppleron cooling.

The theoretical and experimental works so far have been concerned with average behavior of atoms in standing-wave fields. However, the complete quantum dynamics of an atom is not only determined by quantities like dipole moments and populations, but also by fluctuations [6] in such quantities. In particular, the spectrum

of the fluorescence produced by atoms is useful in understanding the role of quantum fluctuations. With this in view we study the spectral features of the radiation produced by an atomic beam in a standing wave field. The organization of this paper is as follows: In Sec. II we show how the calculation of spectrum produced by an atom in a bichromatic field can be adopted for the standing-wave case. In Sec. III we present numerical results. We identify the positions of Dopplerons. In Sec. IV we present perturbative and nonperturbative methods to understand the numerical results of Sec. III.

II. SPECTRUM OF RESONANCE FLUORESCENCE

Consider a two-level atom with excited and ground states denoted, respectively, by $|1\rangle$ and $|0\rangle$ and separated by frequency ω_0 . The atom interacts with a standing wave field

$$\mathbf{E} = \epsilon [\cos(\mathbf{k}_l \cdot \mathbf{r} - \omega_l t) + \cos(\mathbf{k}_l \cdot \mathbf{r} + \omega_l t)]. \quad (2.1)$$

For an atom moving with velocity \mathbf{v} , the field at the position of the atom can be written as a sum of two traveling waves

$$\mathbf{E}(\mathbf{v}t, t) = \frac{\epsilon}{2} e^{-i\omega_2 t} + \frac{\epsilon}{2} e^{-i\omega_1 t} + \text{c.c.}, \quad (2.2)$$

where

$$\omega_1 = \omega_l - D, \quad \omega_2 = \omega_l + D, \quad D = \mathbf{k}_l \cdot \mathbf{v}. \quad (2.3)$$

Thus the calculation of the spectra in a standing-wave field is basically the calculation of the spectra in a bichromatic field, which has been extensively studied [7,8]. However, in most of the previous studies one concentrated on the case of *atomic frequency on resonance with the central frequency* of the fully modulated field [9], whereas for the study of Dopplerons one has to consider situations where the detuning $\Delta = \omega_0 - \omega_l \neq 0$ [cf. Eq. (1.1)]. Thus new features will emerge that were not contained in

previous studies. For the calculation of the spectrum we follow the method of Agarwal *et al.* [7]. We recall the basic equations from their work so that the paper is self-contained. The optical Bloch equations for the polarization and inversion can be written in the matrix form as

$$\frac{\partial \phi}{\partial t} = \mathbf{M}\phi + (\mathbf{M}_+ e^{-i\Omega t} + \mathbf{M}_- e^{i\Omega t})\phi + I, \quad (2.4)$$

where

$$\begin{aligned} \Omega &= \omega_1 - \omega_2, \quad \phi_1 = \langle S^+(t) \rangle = \rho_{01}, \\ \phi_2 &= \langle S^-(t) \rangle = \rho_{10}, \quad \phi_3 = \langle S^z(t) \rangle = \rho_{11} - \rho_{00}. \end{aligned} \quad (2.5)$$

Here S^\pm are the dipole-moment operators and S^z is the inversion operator. The nonzero elements of the matrices $\mathbf{M}, \mathbf{M}_\pm$ are

$$\begin{aligned} M_{11} &= M_{22}^* = \left[i\Delta_2 - \frac{1}{T_2} \right], \quad M_{33} = -1/T_1, \\ M_{13} &= M_{23}^* = -M_{31}^*/2 = -M_{32}/2 = ig^*/2, \\ (M_+)_{23} &= -(M_+)_{31}/2 = -ig/2, \\ (M_-)_{13} &= -(M_-)_{32}/2 = ig^*/2, \\ I_3 &= \eta/T_1, \end{aligned} \quad (2.6)$$

where $\Delta_2 = \omega_0 - \omega_2$, T_1 and T_2 are, respectively, the longitudinal and transverse relaxation constants, η is the population inversion in the absence of the applied field, and g is the Rabi frequency of the field defined by $(\mathbf{d} \cdot \bar{\mathbf{e}}/\hbar)$. Equation (2.4) is written in a frame rotating with frequency ω_2 .

The spectral features of fluorescence are obtained from the dipole-dipole correlation function. This correlation function can be obtained from (2.4) and the knowledge of the correlation matrix $\Phi(t + \tau, t)$ with components

$$\begin{aligned} \Phi_1(t + \tau, t) &= \langle S^+(t + \tau)S^-(t) \rangle - \langle S^+(t + \tau) \rangle \langle S^-(t) \rangle, \\ \Phi_2(t + \tau, t) &= \langle S^-(t + \tau)S^-(t) \rangle - \langle S^-(t + \tau) \rangle \langle S^-(t) \rangle, \\ \Phi_3(t + \tau, t) &= \langle S^z(t + \tau)S^-(t) \rangle - \langle S^z(t + \tau) \rangle \langle S^-(t) \rangle. \end{aligned} \quad (2.7)$$

Using the quantum-regression theorem, one can prove that the matrix Φ satisfies Eq. (2.4) with $I=0$ and $\partial/\partial t \rightarrow \partial/\partial \tau$, $e^{\pm i\Omega t} \rightarrow e^{\pm i\Omega(t + \tau)}$. The time dependence of $\phi(t)$ and $\Phi(t + \tau, t)$ is of the form

$$\begin{aligned} \phi(t) &= \sum_{j=-\infty}^{\infty} \phi^{(j)}(t) e^{-ij\Omega t}, \\ \Phi(t + \tau, t) &= \sum_{j=-\infty}^{\infty} \Phi^{(j)}(\tau) e^{-ij\Omega(t + \tau)}. \end{aligned} \quad (2.8)$$

Furthermore, the steady-state inelastic $S_{in}(\omega)$ and elastic components of the spectrum can be obtained as follows:

$$S_{in}(\omega) = \hat{\Phi}_1^{(0)}[i(\omega - \omega_2)] + c.c., \quad (2.9)$$

$$S_{el}(\omega) = \sum_{j=-\infty}^{\infty} \delta(\omega - \omega_2 + j\Omega) |\phi_1^{(j)}|^2, \quad (2.10)$$

where $\phi_1^{(j)}$ is the steady-state limit of $\phi^{(j)}(t)$. Note further that

$$I_{el} = \int S_{el}(\omega) d\omega = \sum_{j=-\infty}^{\infty} |\phi_1^{(j)}|^2. \quad (2.11)$$

The total intensity of fluorescence is proportional to the population in the excited state

$$I \propto \rho_{11}(t) = [\phi_3(t) + 1]/2. \quad (2.12)$$

The inelastic component of fluorescence in the steady state is equal to

$$I_{in} = I - I_{el} = \frac{1}{2}(1 + \phi_3^{(0)}) - \sum_{j=-\infty}^{\infty} |\phi_1^{(j)}|^2. \quad (2.13)$$

The coupled equations for $\phi^{(j)}, \Phi^{(j)}$ are solved using continued-fraction methods [10]. We discuss the numerical results in Sec. III.

III. NUMERICAL RESULTS

In this section we discuss in detail the spectral features of the fluorescence produced by atoms in a standing-wave field. We consider the case of radiative relaxation so that $T_2 = 2T_1$, $\eta = -1$. We present results for a range of values of the parameters such as the detuning of the field and the intensity of the field.

In Fig. 1 we show the behavior of the total intensity of fluorescence as a function of the Doppler shift $\mathbf{k}_l \cdot \mathbf{v} T_1 \equiv DT_1$. We also exhibit the elastic component of the fluorescence. We find a number of peaks (dips) in the total intensity (I_{el}). These peaks or dips correspond exactly to Doppleron resonances given by the modification of (1.1) due to the large intensity of the standing-wave field. Note that for the first Doppleron resonance the inversion is zero since the total intensity is equal to $\frac{1}{2}$. It may be added that these Doppleron resonances are the analog of the subharmonic Rabi resonances [10–12], which have been extensively studied experimentally [9,12] and theoretically [10,11], particularly using fully modulated pump fields. For the parameters of Fig. 1, these Doppleron resonances occur at $DT_1 = 25.12, 11.25, 6.83, 4.82, 3.28$, etc. The recent experiments [4,5] establish the existence of these Doppleron resonances in the

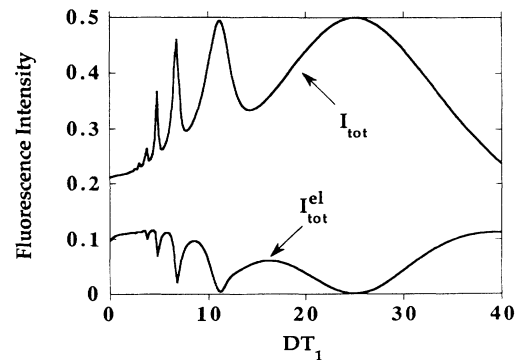


FIG. 1. Total intensity (and its elastic part) of fluorescence as a function of the Doppler shift DT_1 for $gT_1 = \Delta T_1 = 20$.

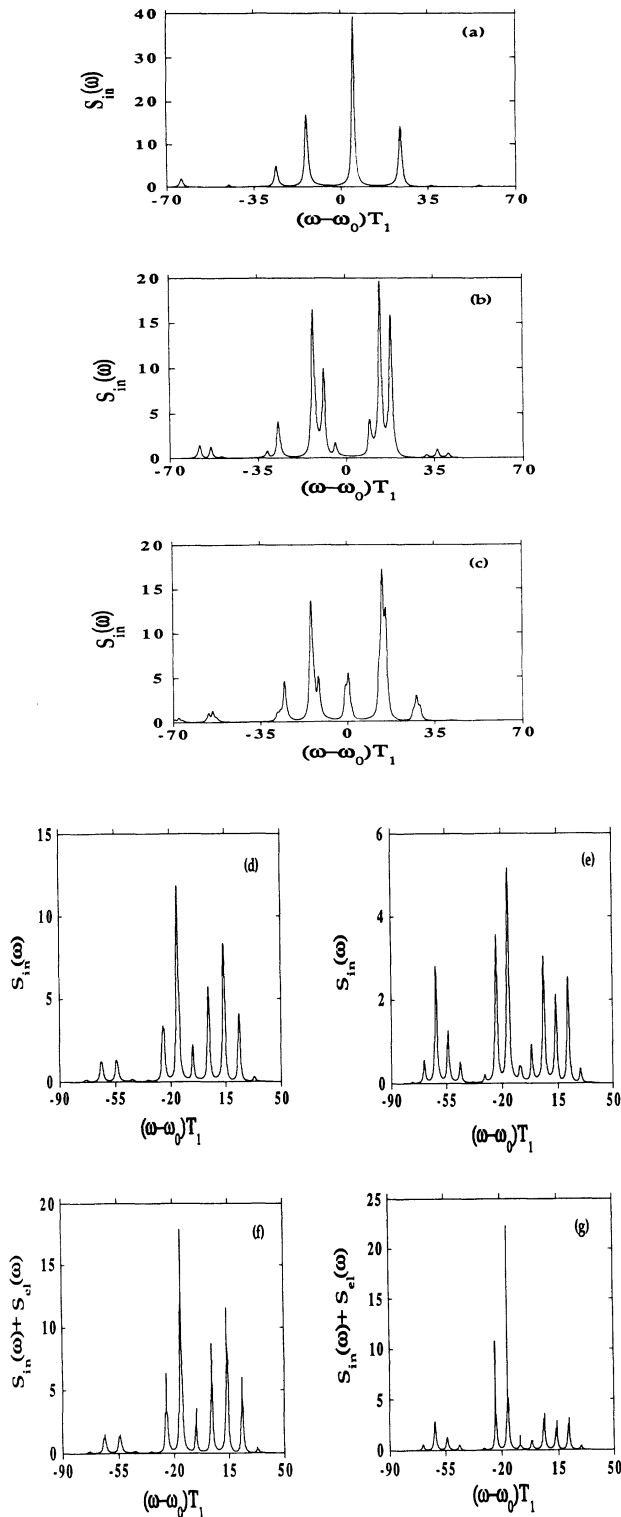


FIG. 2. Spectrum of fluorescence $S_{in}(\omega)$ as a function of $(\omega - \omega_0)T_1$ for the same parameters as in Fig. 1. These spectra are taken at different Doppler resonances, which according to Fig. 1 occur at $DT_1 = 25.12, 11.25, 6.83, 4.82, 3.82$, etc. Parts (a)–(e) correspond, respectively, to these Doppler resonances. In parts (f) and (g) we have also shown elastic peaks that have been obtained by averaging the spectra, Eq. (2.10), over the detector linewidth taken to be $0.01/T_2$.

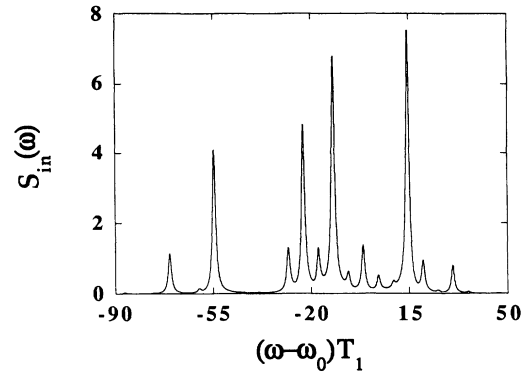


FIG. 3. Inelastic spectra when one is away from any of the Doppler resonances. The parameters are chosen as $gT_1 = \Delta T_1 = 20, DT_1 = 8$.

total fluorescence produced by an atom in a standing-wave field. It is also to be noted in Fig. 1 that higher-order Doppler resonances have subnatural linewidths; for example, the fourth resonance has a linewidth of about $T_1/3$.

We next show in a series of figures the spectral features of the fluorescence under *conditions of resonance*. By resonance we understand that the parameters like the detuning, the Doppler shift, and the intensities are such that the condition for a given Doppler resonance is satisfied. Figure 2 shows the sensitive dependence of the spectral features on the order of the Doppler resonance. In some cases [Figs. 2(f) and 2(g)] we have also shown the elastic spectra. According to Eq. (2.10) the peaks in the elastic spectra occur at

$$(\omega - \omega_0)T_1 = -\Delta T_1 + (2n + 1)DT_1, \quad (3.1)$$

where n is an integer and Δ is the atom laser detuning (defined by setting $D = 0$). It may be noticed that the positions of the elastic peaks are independent of the field intensity, whereas the inelastic peaks do depend on the Rabi frequency of the pump. In Fig. 3 we exhibit the spectra when the conditions for Doppler resonances are not satisfied. So these in a sense correspond to off-

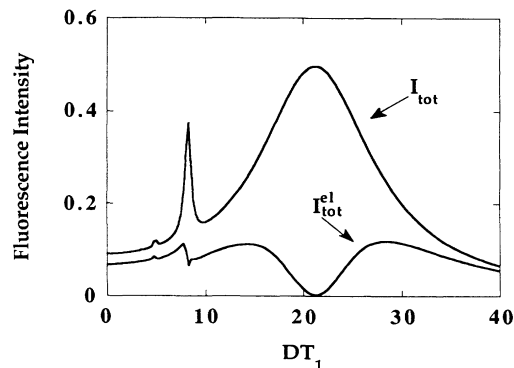


FIG. 4. Same as in Fig. 1 but now the Rabi frequency of the pump field is smaller $gT_1 = 10$. The Doppler resonances occur at $DT_1 = 21.25, 8.22, 4.91$, etc.

resonant spectra. We also show the nature of the spectra when the Rabi frequency is smaller than the atom-field detuning. The elastic component of the total fluorescence exhibits a behavior (Fig. 4) different from that in Fig. 1. One, for example, sees that at the third Doppleron resonance both I and I_{el} exhibit maxima. Figure 5 gives the spectra at first, second, and third Doppleron resonances. We will be able to understand some of these spectra in terms of a perturbative approach in the next section. It is interesting to observe that at the second Doppleron resonance each peak splits into two.

IV. INTERPRETATION OF THE SPECTRA IN A STANDING-WAVE FIELD

In this section we explain the spectral features of Sec. III. We first give a qualitative discussion and then present a quantitative approach. Let us consider Mollow spectra [6] obtained if the atom were interacting with two beams and if the interaction between beams were unimportant. In such a case we expect resonances at

$$\omega^{(1)} = \omega_0 - (\Delta - D), \quad \omega_0 - (\Delta - D) \pm [g^2 + (\Delta - D)^2]^{1/2}, \quad (4.1)$$

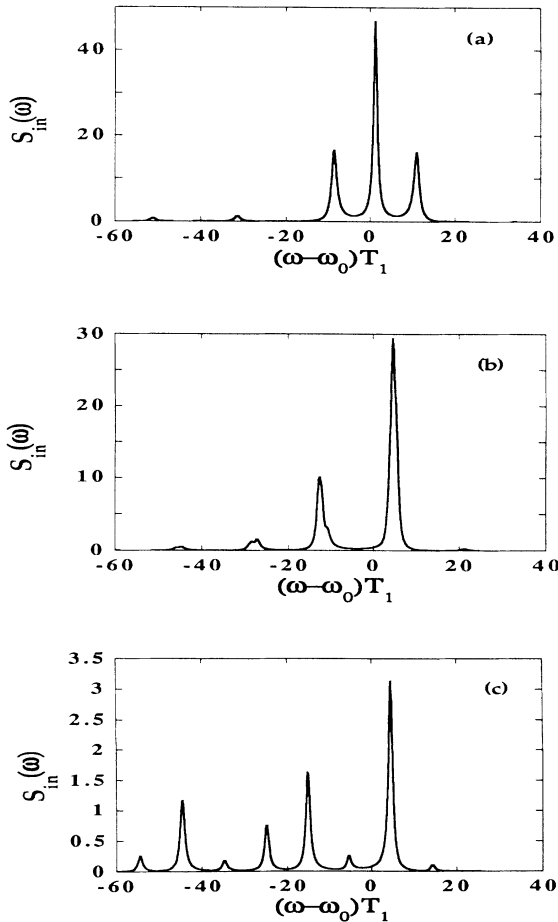


FIG. 5. Spectrum of fluorescence $S_{in}(\omega)$ for the same parameters as in Fig. 4. Parts (a)–(c) correspond to different Doppleron resonances, i.e., to $DT_1 = 21.25, 8.22,$ and 4.91 .

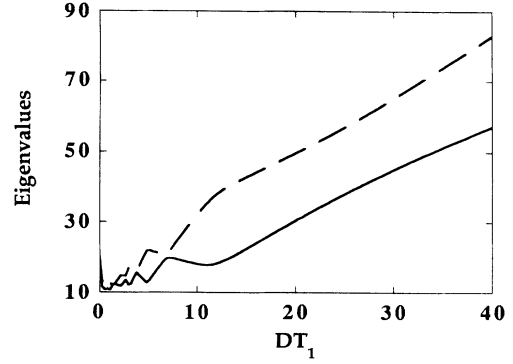


FIG. 6. Plot of eigenvalues α_1 and α_2 as a function of the Doppler shift D for $gT_1 = \Delta T_1 = 20$.

$$\omega^{(2)} = \omega_0 - (\Delta + D), \quad \omega_0 - (\Delta + D) \pm [g^2 + (\Delta + D)^2]^{1/2}. \quad (4.2)$$

Now imagine that $\Delta \approx D$, then the field ω_1 is close to resonance, whereas the field ω_2 is away from resonance. Thus one can imagine that ω_2 will perturb the spectra produced by ω_1 . This perturbation can be shown [13] to produce fluorescence at $\omega^{(1)} \pm 2nD$ where n is an integer. Similarly, one can produce fluorescence at $\omega^{(2)} \pm 2nD$. The spectral positions in Fig. 5 can be explained by these considerations. The situation gets more complicated for higher-order Doppleron resonances or for higher intensities of the pump. In such cases we have to calculate the spectral positions by Floquet analysis. To do this we consider the interaction Hamiltonian of the atom in the field (2.2). We write it in the rotating-wave approximation,

$$\mathcal{H} = \omega_0 \frac{S^z}{2} - \frac{g}{2} [S^+ (e^{-i(\omega_1 - D)t} + e^{-i(\omega_1 + D)t}) + \text{c.c.}], \quad (4.3)$$

which in the frame rotating with frequency $\omega_2 = \omega_1 + D$ becomes

$$\mathcal{H} = \frac{\Delta_2 S^z}{2} - \frac{g}{2} [S^+ (e^{2iDt} + 1) + \text{c.c.}], \quad \Delta_2 = \omega_0 - \omega_1 - D. \quad (4.4)$$

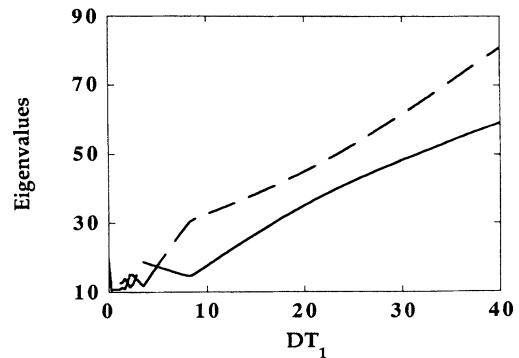


FIG. 7. Same as in Fig. 6, but now the Rabi frequency is small $gT_1 = 10$.

TABLE I. The eigenvalues of \mathcal{H} or the Floquet matrix and the transition frequencies $\omega^{(1)}$, $\omega^{(2)}$, and $\omega^{(3)}$ for different Doppleron resonances and for the nonresonant case ($DT_1=8$) and for $gT_1=\Delta T_1=20$.

DT_1	$(\alpha_1-\alpha_2)T_1$	$\omega^{(1)}T_1$	$\omega^{(2)}T_1$	$\omega^{(3)}T_1$
25.12	19.01	$5.12+50.24n$	$24.13+50.24n$	$-13.89+50.24n$
11.25	4.33	$-8.75+22.50n$	$-13.08+22.50n$	$-4.41+22.50n$
6.83	1.50	$-13.17+13.66n$	$-11.66+13.66n$	$-14.67+13.66n$
3.82	0.60	$-16.18+7.64n$	$-15.57+7.64n$	$-16.78+7.64n$
8.00	5.37	$-12.00+16.00n$	$-16.62+16.00n$	$-17.37+16.00n$

For the purpose of finding the eigenvalues of the Floquet matrix one can either quantize [14] the time dependence $e^{\pm ik_1 vt}$ or rewrite the Schrödinger equation as

$$\frac{id\psi^{(n)}}{dt} = 2Dn\psi^{(n)} + \left[\Delta_2 \frac{S^z}{2} - \frac{g}{2}(S^+ + S^-) \right] \psi^{(n)} - \frac{g}{2}S^+\psi^{n-1} - \frac{g}{2}S^-\psi^{n+1}, \quad (4.5)$$

where

$$\psi^{(n)}(t) = e^{-2iDnt}\psi(t). \quad (4.6)$$

Let us denote the two components $\psi_1^{(n)}, \psi_0^{(n)}$ of the column matrix $\psi^{(n)}$ as the components of an infinite dimensional ψ in terms of the states $|1, n\rangle$ and $|0, n\rangle$. We can now write Eq. (4.5) in matrix form. The matrix, which needs to be diagonalized, is

$$\mathcal{H} - 2nDI = \begin{matrix} & \dots & |1, n-1\rangle & |0, n-1\rangle & |1, n\rangle & |0, n\rangle & |1, n+1\rangle & |0, n+1\rangle & \dots \\ \begin{matrix} \vdots \\ |1, n-1\rangle \\ |0, n-1\rangle \\ |1, n\rangle \\ |0, n\rangle \\ |1, n+1\rangle \\ |0, n+1\rangle \\ \vdots \end{matrix} & \left[\begin{array}{cccccccc} \ddots & & & & & & & & \ddots \\ \dots & \vdots & & & \vdots & \vdots & \vdots & \vdots & \dots \\ \dots & \frac{1}{2}\Delta_2 - 2D & & A & 0 & 0 & 0 & 0 & \dots \\ \dots & A & & -\frac{1}{2}\Delta_2 - 2D & A & 0 & 0 & 0 & \dots \\ \dots & 0 & & A & \frac{1}{2}\Delta_2 & A & 0 & 0 & \dots \\ \dots & 0 & & 0 & A & -\frac{1}{2}\Delta_2 & A & 0 & \dots \\ \dots & 0 & & 0 & 0 & A & \frac{1}{2}\Delta_2 + 2D & A & \dots \\ \dots & 0 & & 0 & 0 & 0 & A & -\frac{1}{2}\Delta_2 + 2D & \dots \\ \dots & \vdots & & \vdots & \vdots & \vdots & \vdots & \vdots & \ddots \end{array} \right] \end{matrix}, \quad (4.7)$$

where

$$A = -\frac{g}{2}. \quad (4.8)$$

The eigenvalues of the matrix \mathcal{H} are

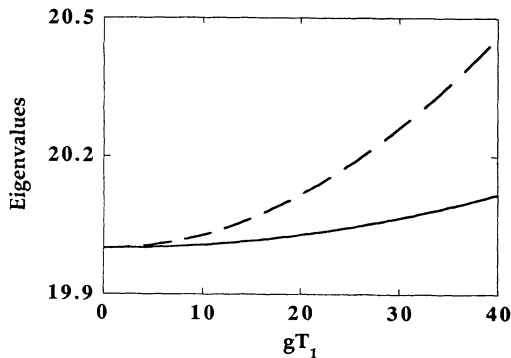


FIG. 8. Eigenvalues as a function of the Rabi frequency of the pump field for $DT_1=10$, $\Delta T_1=20$.

$$\lambda^{(1)} = 2nD + \alpha_1, \quad \lambda^{(2)} = 2nD + \alpha_2. \quad (4.9)$$

The behavior of α_1 and α_2 is shown in Figs. 6–9 for two different values of the Rabi frequency of the pump field. Figure 8 (9) gives the behavior of α_1 and α_2 as a function of Rabi frequency (detuning of the field). The spectral features can be obtained from (4.9). The transition frequencies are

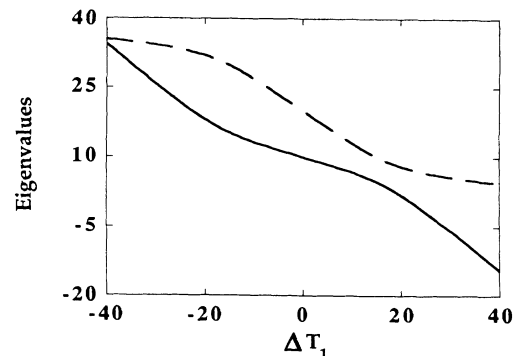


FIG. 9. Eigenvalues as a function of the detuning ΔT_1 for $gT_1=20$, $DT_1=10$.

$$\begin{aligned}
\omega &= \omega_0 - \Delta_2 + 2nD \\
&= \omega_0 - \Delta_2 + 2nD + \alpha_1 - \alpha_2 \\
&= \omega_0 - \Delta_2 + 2nD - \alpha_1 + \alpha_2 .
\end{aligned} \tag{4.10}$$

Note that if the pump is on resonance, i.e., $\Delta=0$, then $\alpha_1=\alpha_2=0$ and the peak positions are independent of the field intensity. An interesting consequence of this is that the field inhomogeneity does not broaden the spectral peaks if $\Delta=0$.

The spectral positions in Figs. 2, 3 and 5 can be understood in terms of (4.10). For example, for $gT_1=\Delta T_1=20$, the transition frequencies are given in Table I. These values match very well the spectral positions in Figs. 2, 3, and 5. However, for $DT_1=3.82$ the peaks are not resolved [Fig. 2(e)] since the numerically

evaluated spectra use $1/T_1=1$. For $DT_1=6.83$, the peaks are just resolvable [Fig. 2(d)] [15].

Thus in conclusion we have shown how the spectral features in a standing-wave field depend on the intensity and detuning of the field. We have shown how the spectral features depend on the Doppleron resonance under consideration. We further showed how the peak positions follow from the structure of the dressed states in a standing-wave field.

ACKNOWLEDGMENT

One of us (G.S.A.) thanks the National Science Foundation for Grant No. INT 9100685, which led to this collaboration.

-
- [1] S. M. Freund, M. Römheld, and T. Oka, *Phys. Rev. Lett.* **35**, 1497 (1975); J. Read and T. Oka, *ibid.* **38**, 67 (1977).
- [2] E. Kyröla and S. Stenholm, *Opt. Commun.* **22**, 123 (1977).
- [3] J. H. Shirley, *Phys. Rev.* **138**, B979 (1965); C. Cohen-Tannoudji, in *Cargèse Lectures in Physics*, edited by M. Levy (Gordon and Breach, New York, 1968), Vol. 2, p. 347.
- [4] J. J. Tollett, J. Chen, J. G. Story, N. W. M. Ritchie, C. C. Bradley, and R. G. Hulet, *Phys. Rev. Lett.* **65**, 559 (1990).
- [5] N. P. Bigelow and M. G. Prentiss, *Phys. Rev. Lett.* **65**, 555 (1990).
- [6] B. R. Mollow, *Phys. Rev.* **188**, 1969 (1969).
- [7] G. S. Agarwal, Y. Zhu, D. J. Gauthier, and T. W. Mossberg, *J. Opt. Soc. Am. B* **8**, 1163 (1991).
- [8] For other approaches for the calculation of the spectra in a bichromatic field, see, for example, M. Wilkens and K. Rzazewski, *Phys. Rev. A* **40**, 3164 (1989); M. K. Kumari and S. P. Tewari, *ibid.* **41**, 5273 (1990); H. Fredhoff and Z. Chen, *ibid.* **41**, 6013 (1990); B. Blind, P. R. Fontana, and P. Thomann, *J. Phys. B* **13**, 2728 (1980); M. A. Newbold and G. J. Salamo, *Phys. Rev. A* **22**, 2098 (1980).
- [9] Y. Zhu, Q. Wu, A. Lezama, D. J. Gauthier, and T. W. Mossberg, *Phys. Rev. A* **41**, 6547 (1990).
- [10] G. S. Agarwal and N. Nayak, *J. Opt. Soc. Am. B* **1**, 164 (1984); *Phys. Rev. A* **33**, 391 (1986); *J. Phys. B* **19**, 3385 (1986).
- [11] W. M. Ruyten, *Opt. Lett.* **14**, 506 (1989); *Phys. Rev. A* **40**, 1447 (1989); *J. Opt. Soc. Am. B* **6**, 1796 (1989).
- [12] S. Chakmakjian, K. Koch, and C. R. Stroud, Jr., *J. Opt. Soc. Am. B* **5**, 2015 (1988); S. Papademetriou, S. Chakmakjian, and C. R. Stroud, Jr., *ibid.* (to be published).
- [13] G. S. Agarwal, *J. Opt. Soc. Am. B* **5**, 149 (1988).
- [14] T. Yabuzaki, S. Nakayama, Y. Murakami, and T. Ogawa, *Phys. Rev. A* **10**, 1955 (1974).
- [15] In principle, it is also possible to calculate the full spectra using the above matrix (4.7). However, this requires the knowledge of the eigenfunctions of (4.7). This makes it rather cumbersome and so we do not attempt it here.